WSR-88D Tornado Intensity Estimates. Part II: Real-Time Applications to Tornado Warning Time Scales

BRYAN T. SMITH,[a] RICHARD L. THOMPSON,[a] DOUGLAS A. SPEHEGER,[b] ANDREW R. DEAN,[a]
CHRISTOPHER D. KARSTENS,[a] AND ALEXANDRA K. ANDERSON-FREY[c]

[a] *NOAA/NWS/NCEP, Storm Prediction Center, Norman, Oklahoma*
[b] *NOAA/NWS/Weather Forecast Office, Norman, Oklahoma*
[c] *Cooperative Institute for Mesoscale Meteorological Studies, University of Oklahoma, Norman, Oklahoma*

ABSTRACT: A sample of damage-surveyed tornadoes in the contiguous United States (2009–17), containing specific wind speed estimates from damage indicators (DIs) within the Damage Assessment Toolkit dataset, were linked to radar-observed circulations using the nearest WSR-88D data in Part I of this work. The maximum wind speed associated with the highest-rated DI for each radar scan, corresponding 0.5° tilt angle rotational velocity V_{rot}, significant tornado parameter (STP), and National Weather Service (NWS) convective impact-based warning (IBW) type, are analyzed herein for the sample of cases in Part I and an independent case sample from parts of 2019–20. As V_{rot} and STP both increase, peak DI-estimated wind speeds and IBW warning type also tend to increase. Different combinations of V_{rot}, STP, and population density—related to ranges of peak DI wind speed—exhibited a strong ability to discriminate across the tornado damage intensity spectrum. Furthermore, longer duration of high V_{rot} (i.e., ≥70 kt) in significant tornado environments (i.e., STP ≥ 6) corresponds to increasing chances that DIs will reveal the occurrence of an intense tornado (i.e., EF3+). These findings were corroborated via the independent sample from parts of 2019–20, and can be applied in a real-time operational setting to assist in determining a potential range of wind speeds. This work provides evidence-based support for creating an objective and consistent, real-time framework for assessing and differentiating tornadoes across the tornado intensity spectrum.

KEYWORDS: Supercells; Tornadoes; Storm environments; Radars/Radar observations; Forecasting techniques; Operational forecasting

1. Introduction

Blair and Leighton (2014) noted the need for robust, scientific guidance for real-time tornado intensity estimates in their assessment of event confirmation in NWS warnings and statements across the central CONUS from 2007–11. A few NWS local forecast offices began issuing experimental impact-based warnings (IBW; Wagenmaker et al. 2014) in 2012 for severe thunderstorms and tornadoes. The practice of issuing IBWs underwent increasing adoption in phases by additional NWS local forecast offices and became a nationwide practice in 2016. The IBWs are intended to convey the potential impact to life and property within the disseminated warning text, based on the forecaster's subjective estimate of the threat posed by a tornado. Forecasts of tornado intensity remain a challenge within the context of tornado warning time scales. Forecast lead time with skill relies on interpretation of full volumetric WSR-88D data (e.g., Gibbs and Bowers 2019), as well as temporal trends in combinations of rotational characteristics and near-storm environment (Baerg et al. 2020). Forecasts of weak tornadoes [enhanced Fujita (EF) scale (EF0–EF1)] on the time scale of tornado warnings remain difficult. Work to date has focused primarily on discrimination between weak and strong tornadoes (e.g., Kingfield and LaDue 2015), lead time to the onset of EF2+ tornado damage (Gibbs and Bowers 2019), or the potential for stronger tornadoes with wider

mesocyclones (Sessa and Trapp 2020). Variations in tornado intensity *within* tornado warning time scales (beyond the EF2+ discrimination) have not received as much attention.

Recent studies [e.g., Thompson et al. 2012, 2017, hereafter T17; Smith et al. 2015; Cohen et al. 2018] provided empirical evidence of variations in tornado damage-based intensity as a function of near-storm environmental conditions and storm-scale rotation strength. More specifically, the significant tornado parameter (STP;[1] Thompson et al. 2012) and manually determined 0.5° tilt angle maximum rotational velocity V_{rot} from the nearest single-site WSR-88D, served as single-variable proxies for the near-storm environmental conditions, and storm-scale rotation strength, respectively. As discussed in Smith et al. (2020, hereafter Part I) of this work, tornadoes are not resolved explicitly in WSR-88D data. Per high-resolution mobile Doppler radar observations, mesocyclone signatures resolvable in WSR-88D data do not necessarily vary in tandem with tornado intensity (French et al. 2013, 2014; Marquis et al. 2016; Bluestein et al. 2019), and rapid fluctuations in tornado intensity can occur on spatiotemporal scales unresolvable in WSR-88D data. Some of the highest ground-relative wind speeds in well-sampled tornadoes are produced by embedded subvortices, which can vary on the order of tens of meters and tens of seconds (e.g., French et al. 2013; Wakimoto et al. 2016; Bluestein et al. 2018, 2019). Ideally, tornado damage swaths

---

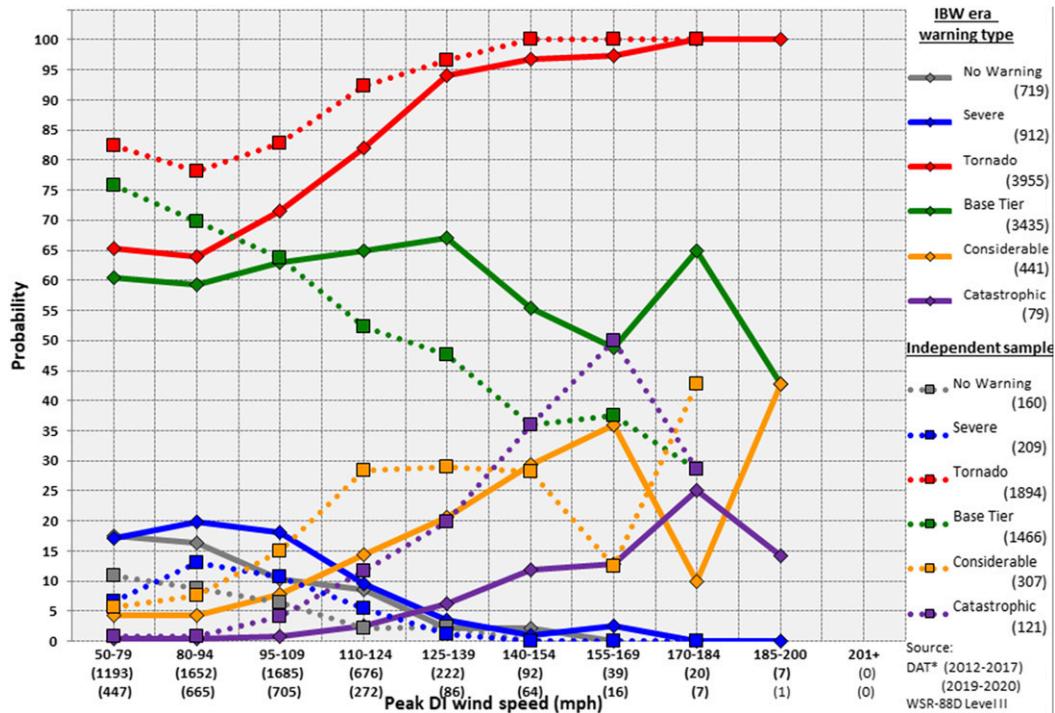[1] STP effective-layer calculation with convective inhibition.

FIG. 1. Probability of impact-based warning (IBW) type vs binned wind speeds of peak damage indicators (mph; x coordinate). No warning, severe, and tornado (base-tier tornado, considerable, catastrophic) sum to 100% probability. The 2009–17 data (solid line) vs 2019–20 independent data (dotted line; $1\ \mathrm{mph} = 0.447\ \mathrm{m\,s^{-1}}$).

could be estimated in real time via mobile Doppler radar data, though such data are not available in real time or for the majority of tornadoes across the CONUS.

After the EF scale (WSEC 2006) was implemented to assign wind-engineered intensity estimates to tornado damage in 2007, the Damage Assessment Toolkit (DAT; Camp et al. 2010) was created to digitally archive tornado damage metadata. The National Weather Service (NWS) began the DAT-based data collection effort in 2007 from a few select tornado events. A larger fraction of tornadoes were digitally archived in the DAT as this practice became increasingly adopted by more NWS local forecast offices in recent years.[2] The EF scale contains 28 damage indicators (DIs), each associated with degrees of damage (DoD) indicating a range of possible wind speeds (WSEC 2006).

Smith et al. (2020, hereafter Part I) examined V_{rot} for individual DIs accompanying nearly 3400 tornadoes from 2009 to 2017 across the contiguous United States. Part I provided direct evidence that peak tornado intensity can be estimated on a scan-by-scan basis with WSR-88D data, albeit as a "worst-case scenario," since predicted speeds will frequently exceed the weaker DIs that are ubiquitous within any tornado damage path, especially within portions of a tornado path affecting rural areas with few or no DIs. This work addresses a gap in

quantitative information within NWS tornado warning time scales by developing *diagnostic* applications of the findings of Part I. A tornado damage–estimation matrix—based on combinations of V_{rot}, STP, and population density—provides tornadic wind speed ranges and allows for a real-time, diagnostic assessment of potential tornado damage intensity and accompanying peak DI wind speeds. The relationship between tornado damage intensity information and NWS IBW tornado warnings is discussed, along with an objective approach for applying these findings to better discriminate potential tornado damage intensity in a real-time operational setting, for ongoing tornadoes.

2. Data and methods

a. Tornado data and attribute pairing

The findings of Part I serve as the basis for the potential tornado warning applications described herein. Various distributions of V_{rot} as a function of DIs were considered by Part I, and they ultimately recommended using V_{rot} from individual 0.5° tilt angle WSR-88D scans to estimate peak DI wind speeds with each scan update for ongoing tornadoes. Part I made no attempt to estimate tornado damage path widths or integrated damage areas, which would be necessary to quantify potential tornado impacts. The Part I approach resulted in 7513 0.5° tilt angle scans with accompanying values of V_{rot}, STP, and a peak DI-based wind speed. The type of warning in effect, including no warning, was documented at the time of each 0.5° DI scan

---

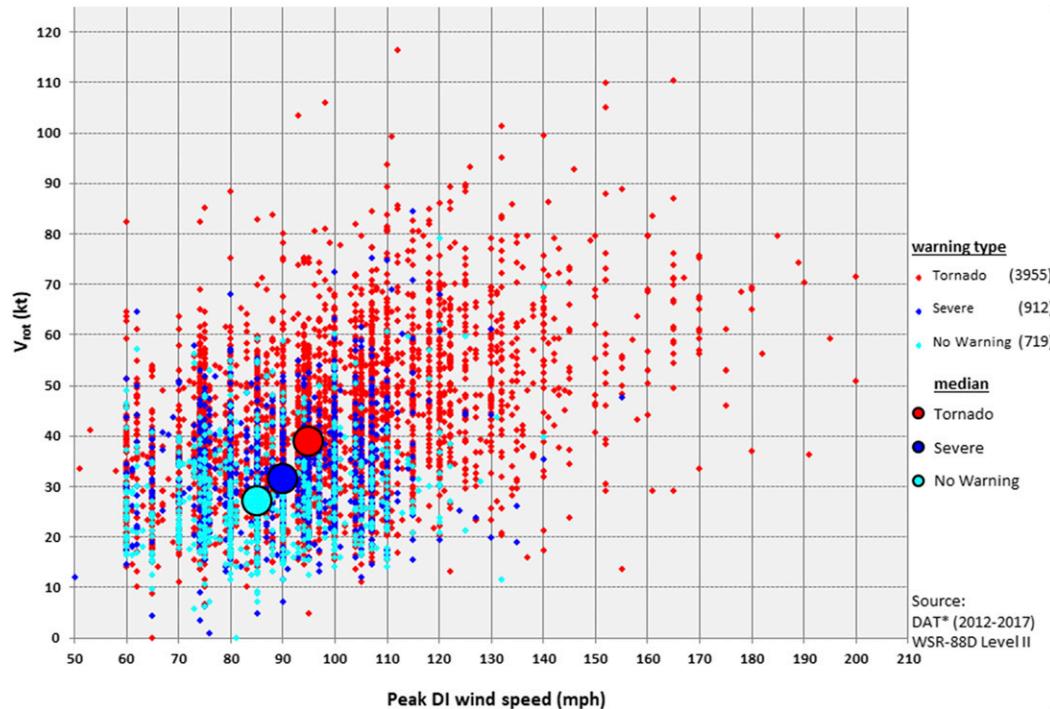[2] DAT became mandated by NWS field offices in 2018, just after the 2009–17 study period.

FIG. 2. Scatterplot of 0.5° DI scans by warning type (no warning, cyan; severe thunderstorm, blue; tornado, red) of peak DI wind speed (mph; *x* coordinate) vs V_{rot} (kt; *y* coordinate) during the IBW era. The large circles represent the median values of DI wind speed and V_{rot} for each warning type (1 mph = 0.447 m s^{-1}, 1 kt = 0.514 m s^{-1}).

for each tornado. Prior to the IBW era, four categories (i.e., no warning, severe thunderstorm warning, tornado warning, and tornado emergency) were assigned. Since IBW was adopted in phases beginning in April 2012, this analysis will only include warnings from IBW-issuing NWS forecast offices during the IBW era through 2017, which reduces the number of 0.5° DI scans analyzed from 7513 to 5586.

An independent test sample (13 024 initial DIs associated with 2263 0.5° radar scans during 637 tornadoes) was developed using DAT-archived tornado events from January–May 2019, along with 10 additional tornadoes from late 2019 and April 2020. In addition to NWS warning type in effect at the time of each 0.5° scan, gridded population density data (~0.5-km resolution) from the 2010 U.S. census were associated with the centroid of each individual V_{rot}, which allows some quantification of the influence of population on tornado intensity estimates. Two mutually exclusive sets of tornadoes grouped by population density (i.e., <20 people km^{-2} and ≥20 people km^{-2}) were analyzed (see section 3e).

b. Kernel density estimation

Following the methodology of Anderson-Frey et al. (2016, 2018), kernel density estimation (KDE; based on a Gaussian kernel) was used to compare the two-dimensional parameter space of V_{rot} and peak DI wind speed by warning type. Statistical significance testing examined the difference between mean values of a given variable (i.e., differences in peak DI wind speed and V_{rot} between the different warning types

during the IBW era). Significance at the $\alpha = 0.05$ level is evaluated using a 10 000-sample bootstrap.

c. Duration

The duration of the 0.5° scans meeting particular criteria was calculated as the time difference between the first scan where criteria were met and the next scan where criteria were no longer met. For example, using the criteria of $V_{rot} \geq 70$ kt and STP80km ≥ 6, if the time of the first scan meeting the criteria was 0000 UTC, the following scans continued to meet the criteria from 0002 to 0006 UTC, and criteria were no longer met at 0008 UTC, the duration meeting criteria was calculated as 0008 UTC minus 0000 UTC, or 8 min. The minimum duration for a single scan meeting criteria would be the time between the scan updates (2 min in the case of the previous example). Duration totals were summed through the entire lifetimes of the tornadoes, with some tornadoes having multiple periods meeting the same criteria.

3. Results

a. Impact-based warnings

Warning type and V_{rot} data during the IBW era were examined for all surveyed tornadoes within the DAT (Fig. 1). Tornadoes were accompanied by tornado warnings (3955 or 71%) for the majority of individual 0.5° DI scans compared to severe thunderstorm (912 or 16%) and no warning (719 or 13%). Tornado warnings also became increasingly probable as peak DI wind speed increased. As the peak DI wind speed
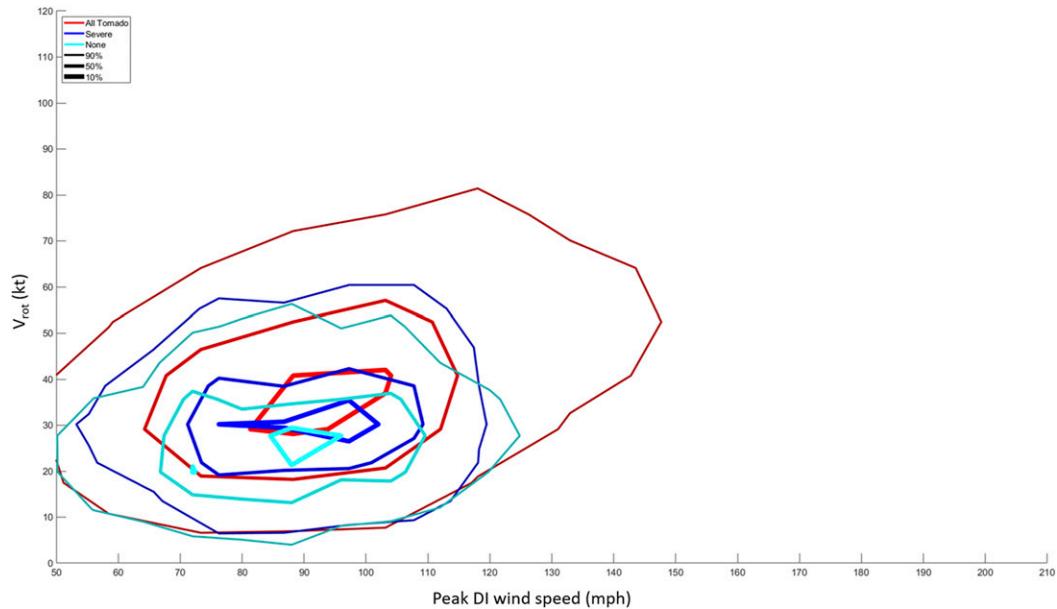
FIG. 3. Kernel density estimation is used to smooth the data for the respective warning type by peak DI wind speed (mph; x coordinate) and V_{rot} (kt; y coordinate). Contours are centered on the point of highest density and contain 10%, 50%, and 90% of the data. Events are contoured by no warning (cyan), severe thunderstorm warning (blue), and tornado warning (red); inner contours are slightly thicker than outer contours (1 mph = 0.447 m s^{-1}, 1 kt = 0.514 m s^{-1}).

increased from weak tornado [i.e., 80–94 mph (36–42 m s^{-1})] to strong tornado [i.e., 125–139 mph (56–62 m s^{-1})], the percentage of tornado warnings valid at the time of each of the 0.5° scans increased from 64%–94%. IBW tornado warnings include a base-tier warning, a considerable warning tag, and a catastrophic warning tag. Comparing five potential options for a warning (i.e., no warning, severe thunderstorm, base-tier tornado, considerable tornado, and catastrophic tornado) in Fig. 1, all three tornado warning types exhibited increasing probabilities as binned peak DI-estimated wind speeds increased from 80–94 mph (36–42 m s^{-1}) to 125–139 mph (56–62 m s^{-1}). However, the most common warning type was the base-tier tornado warning, regardless of peak DI-estimated tornado wind speeds, as discussed in Gibbs and Bowers (2019).

Conversely, as peak DI-estimated wind speeds increased, the probability of no warning and severe thunderstorm warning decreased. The probability for a base-tier tornado warning also decreased for the 140–154 mph (63–69 m s^{-1}) and 155–169 mph (69–76 m s^{-1}) wind speed bins, while considerable and catastrophic warning tag probabilities increased. The sample size is relatively small for 0.5° scans associated with DI-estimated wind speeds ≥ 170 mph (76 m s^{-1}).

The peak DI wind speeds, based on 0.5° DI scans for the independent sample of tornadoes from parts of 2019–20, are also plotted in Fig. 1. During the more recent period of the independent sample, it appears that discrimination of tornado intensity within IBW has improved by some measures. For example, the probabilities of a base-tier tornado warning have increased by 10%–15% for the weakest peak DI wind speeds (50–94 mph), and decreased by roughly the same percentages

in the 125–154-mph range (upper EF2–middle EF3 damage), where sample sizes are still reasonably large. An increase in catastrophic tags for peak DI wind speeds of 125–169 mph (middle EF2–lower EF4 damage) is at the expense of base-tier tornado warnings. On the other hand, the probabilities of considerable and catastrophic tags have roughly doubled for peak DI wind speeds of 110–124 mph (EF1–lower EF2). The source(s) of the changes since 2017 are not known with high confidence, though it is reasonable to assume that NWS training efforts and increased forecaster experience have both contributed positively to warning performance since 2017 (e.g., the training guidelines advanced by Gibbs 2016).

Many of the no-warning 0.5° DI scans were skewed toward weak peak DI wind speeds [i.e., ≤110 mph (49 m s^{-1})] and weak V_{rot} [i.e., ≤35 kt (18 m s^{-1}); Fig. 2]. In contrast, tornado warning 0.5° DI scans were distributed across a much larger range of peak DI wind speed and V_{rot}. NWS warning types were also compared using median (50th percentile) values of peak DI-estimated wind speed and V_{rot} for each warning type. Tornado warnings were characterized by higher median values of peak DI-estimated wind speed [95 mph (42 m s^{-1})] and V_{rot} [39 kt (20 m s^{-1})] than severe thunderstorm and no-warning 0.5° DI scans. Two-dimensional comparisons of warning types were achieved through KDE (which functions similarly to a two-dimensional histogram, without the sharp categorical breaks; Fig. 3). The inner density contour (i.e., 10th percentile) of the tornado and severe thunderstorm warnings overlap some with one another, but not with the tornadoes that were unwarned. Otherwise, the most pronounced difference stemming from Fig. 3 is the extension of the tornado warnings into
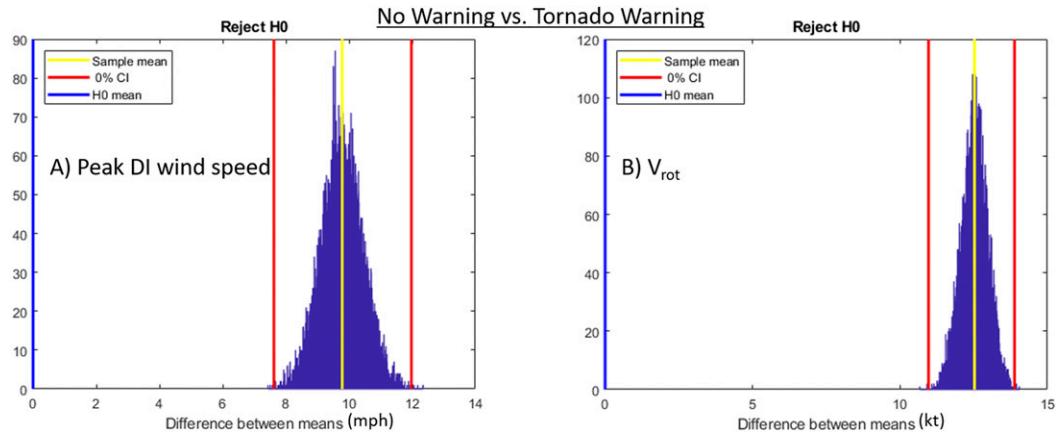
FIG. 4. Histograms comparing no-warning vs tornado warning for each 0.5° tilt angle WSR-88D scan during each tornado. The yellow lines are the actual difference between mean values, and the red lines demarcate the 5% confidence interval of the bootstrap sample built by randomly redistributing the data between the two warning types and then calculating the mean. The blue line at 0 equates to the hypothesis testing [difference of means is zero (i.e., that the two categories are the same)]. (a) Peak DI wind speed (mph; x coordinate) and (b) V_{rot} (kt; x coordinate; 1 mph = 0.447 m s^{-1}, 1 kt = 0.514 m s^{-1}).

the higher V_{rot} and peak DI wind speed parameter space at the 90th percentile. Among no warning, severe thunderstorm, and tornado warnings, all differences in the means for peak DI-estimated wind speed and V_{rot} are statistically significant at $\alpha = 0.05$. The difference of means was largest between no warning and tornado warning, which represented the most practical value (Fig. 4) in discrimination among the three warning types. Discrimination between nontornadic and weakly tornadic storms will remain challenging, as illustrated by the tornado events/peak DI scans with no warning or severe thunderstorm warnings shown in Figs. 3 and 4, and the relatively low tornado probabilities for similarly weak V_{rot} [<30 kt (15 m s^{-1}); T17). Tornado warnings with appropriate lead time require more complete assessments of storm structure/evolution and
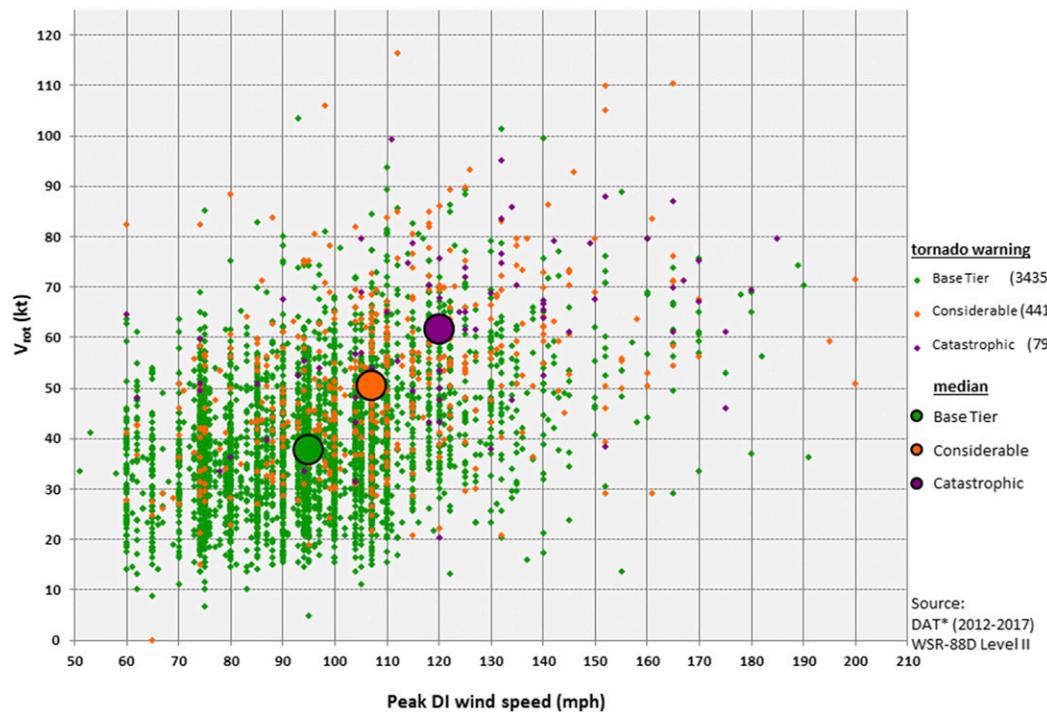

FIG. 5. As in Fig. 2, but for base-tier tornado warning (green), considerable warning tag (orange), and catastrophic tornado warning tag (purple; 1 mph = 0.447 m s^{-1}, 1 kt = 0.514 m s^{-1}).
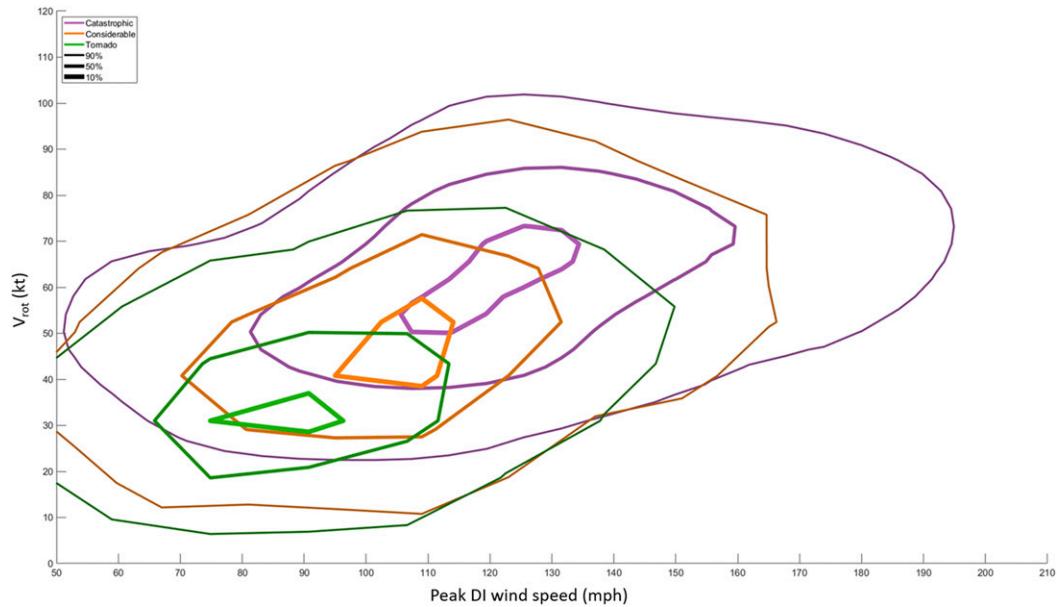
FIG. 6. As in Fig. 3, but for base-tier tornado warning (green), considerable warning tag (orange), and catastrophic tornado warning tag (purple; 1 mph = 0.447 m s⁻¹, 1 kt = 0.514 m s⁻¹).

near-storm environment (e.g., Gibbs and Bowers 2019; Sessa and Trapp 2020; Baerg et al. 2020) than snap shots of V_{rot} alone.

The IBW base-tier tornado warnings displayed a very large range of both peak DI-estimated wind speed [51–191 mph (23–85 m s⁻¹)] and V_{rot} [5–103 kt (3–53 m s⁻¹); Fig. 5]. Catastrophic-tag warnings were more common with ≥120-mph (54 m s⁻¹) peak DI-estimated wind speeds and ≥70-kt (36 m s⁻¹) V_{rot}, and were less common with ≤100-mph (45 m s⁻¹) peak DI-estimated wind speeds and ≤50-kt (26 m s⁻¹) V_{rot}. The median values of the tornado warning types increase almost linearly from base-tier [i.e., 95-mph (42 m s⁻¹) peak DI-estimated wind speed, 38-kt (20 m s⁻¹) V_{rot}], to considerable-tag [107-mph (48 m s⁻¹) peak DI-estimated wind speed, 51-kt (26 m s⁻¹) V_{rot}], and finally to catastrophic-tag [120-mph (54 m s⁻¹) peak DI wind speed, 62-kt (32 m s⁻¹) V_{rot}]. The inner 10% density contours of KDE for base-tier and catastrophic warnings are distinctly offset from each other and minimal overlap exists for the 50% density contour between base-tier and catastrophic-tag tornado warnings (Fig. 6). According to KDE analysis, base-tier warnings are most densely concentrated with the weaker peak DI-estimated wind speeds and V_{rot}, considerable-tag warnings possess stronger peak DI-estimated wind speeds and V_{rot}, and catastrophic-tag warnings display the highest values of peak DI-estimated wind speeds and V_{rot}. The base-tier, considerable-tag, and catastrophic-tag warnings peak DI-estimated wind speed and V_{rot} were compared by warning type and all of their difference of means were statistically significant at $\alpha = 0.05$. As anticipated, the base-tier versus catastrophic-tag warnings yielded the largest difference of means (Fig. 7) for peak DI-estimated wind speed [27 mph (11 m s⁻¹)] and V_{rot} [22 kt (11 m s⁻¹)]. These results suggest that IBW demonstrates some skill in discriminating between the weaker and stronger portions of tornado paths, based on both peak DI wind speeds and V_{rot}.

b. Convective mode

Further tornado damage intensity discrimination appears possible when accounting for convective mode—the median values for peak DI-estimated wind speed and V_{rot} increased from disorganized, to QLCS, to supercell. The disorganized storm type (Smith et al. 2012) includes discrete cells and clusters responsible for landspouts (Brady and Szoke 1989), waterspouts from land/sea-breeze interactions, weak convection associated with tropical cyclones (Edwards et al. 2012), and so-called cold-air funnels. Tornadoes with disorganized storms almost exclusively result in weak damage (EF0–1) with correspondingly weak $V_{rot} < 40$ kt (21 m s⁻¹; Fig. 8), though our sample of tornadoes (and accompanying DIs from damage surveys) with disorganized storms is small compared to supercells and QLCSs. The median values from disorganized storms were substantially weaker for peak DI-estimated wind speed [85 mph (38 m s⁻¹)] and V_{rot} [20 kt (10 m s⁻¹)] than the median values from all IBW warning types, as well as the QLCS and supercell[3] modes (see Fig. 8). QLCS tornadoes clustered in the V_{rot} range of 20–50 kt (10–25 m s⁻¹) with peak DI wind speeds generally ≤110 mph (49 m s⁻¹). Supercells were the dominant mode with $V_{rot} > 50$ kt (25 m s⁻¹) and peak DI-estimated wind speed > 110 mph (49 m s⁻¹), and were exclusive to $V_{rot} \geq 70$ kt and violent (EF4+) tornado damage [i.e., ≥166 mph (74 m s⁻¹)].

c. Quantifying potential tornado damage intensity

Substantial discrimination of peak DI wind speed (Fig. 9) was achieved by exclusive grouping of V_{rot}/STP80km ranges

---

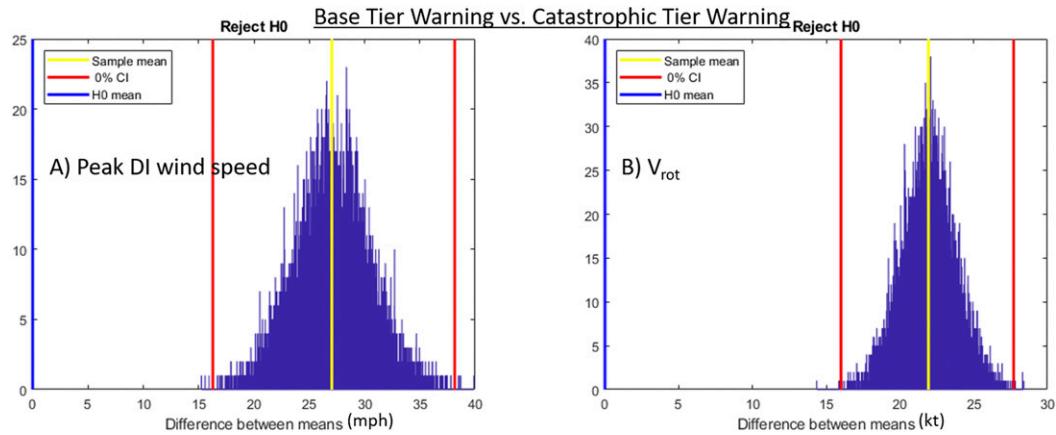[3] Supercell nomenclature used interchangeably with Smith et al.'s (2012) right-moving supercell (RM) definition.

FIG. 7. As in Fig. 4, but for base-tier tornado warning vs catastrophic-tier tornado warning (1 mph = 0.447 m s^{-1}, 1 kt = 0.514 m s^{-1}).

(Figs. 9–11) in order to differentiate peak DI-estimated wind speeds across the tornado intensity spectrum, given the range of peak DI-estimated wind speeds possible for particular values of V_{rot} (e.g., Figs. 2, 5, and 8). Combining the two weakest-magnitude bins of V_{rot} and STP80km (i.e., the green columns on the left side of Fig. 9) resulted in peak DI wind speeds ≤ 110 mph (49 m s^{-1}) for 95% of the individual 0.5° DI scans (Fig. 10). Because the distributions of peak DI wind speeds for the aforementioned two weakest bins of V_{rot}/STP80km were similar (Fig. 9), these cases are grouped in a potential tornado damage intensity class referred to as

level 1 (Figs. 10 and 11). Supercells with weak low-level mesocyclones, QLCSs with weak mesovortices, or disorganized storm modes are common in level 1. Stronger combinations of V_{rot} and STP80km resulted in progressively higher median values of peak DI wind speeds in the level 2–3 range (Fig. 10). Last, the rare combination of $V_{rot} \geq 70$ kt (36 m s^{-1}) and STP80km ≥ 6, yielded a large fraction (44%) of the violent tornado equivalent (EF4–5) 0.5° DI scans in levels 4–5.

Anecdotal evidence prompted the consideration of population density, which corresponds to DI availability. It is hypothesized that DI wind speeds in the upper half of the EF-scale—which
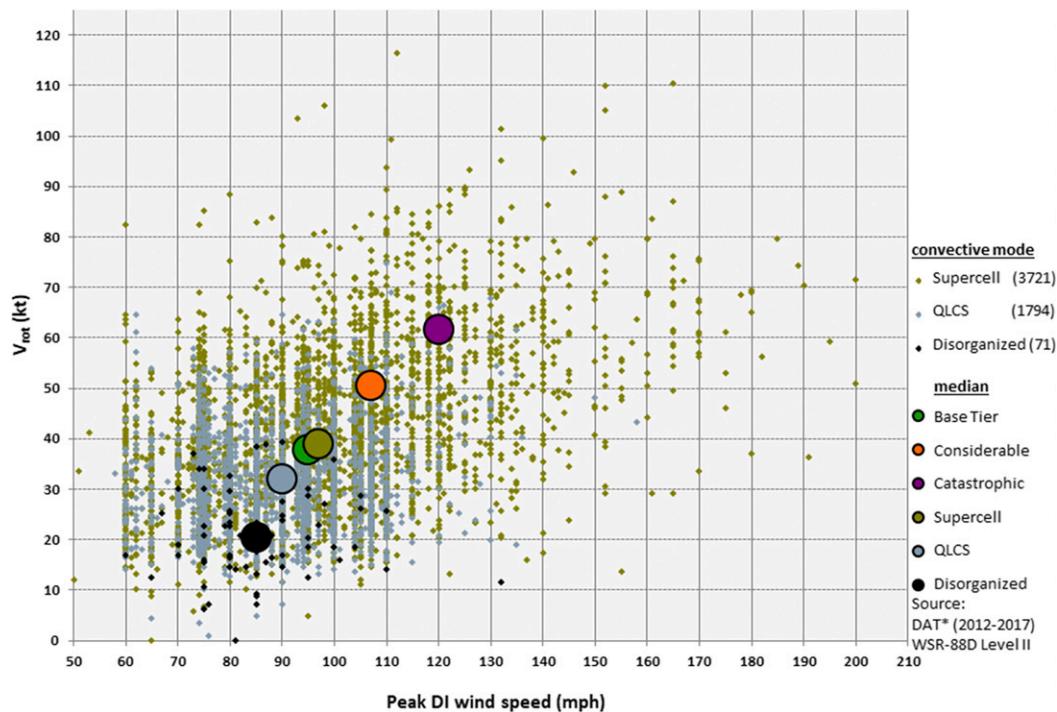

FIG. 8. As in Fig. 5, but for supercell (gold), QLCS (silver), and disorganized convective mode (black; 1 mph = 0.447 m s^{-1}, 1 kt = 0.514 m s^{-1}).
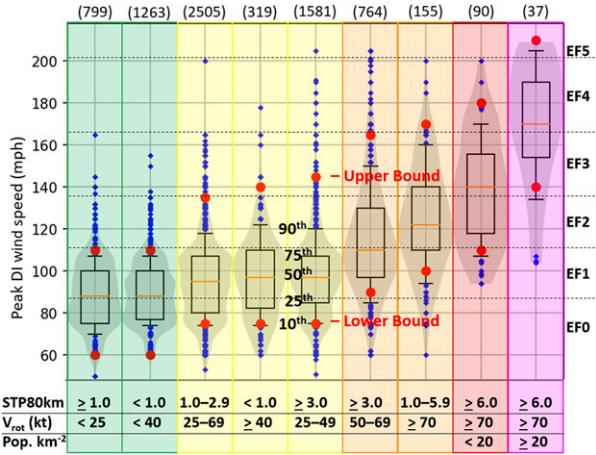
FIG. 9. Violin plots corresponding to rows of criteria in (x axis) vs peak DI wind speed (mph; y axis). The 10th, 25th, 50th, 75th, and 90th percentiles are annotated. The red circles are the lower and upper bounds of the peak DI wind speed damage estimate (WSDE) for each category shown in Fig. 10. The color shading corresponds to levels 1–5 in Fig. 10 (1 mph = 0.447 m s^{-1}, 1 kt = 0.514 m s^{-1}).

disproportionately occur in high-end environments with very strong V_{rot} signatures—combined with population density, may provide utility in discerning wind speed damage ratings. Sutton et al. (2006) examined population density for 49 major U.S. cities and their surrounding exurbia and found each city's exurbia population density was ≥24 people km^{-2} (Minneapolis/St. Paul, Minnesota, had the lowest threshold for exurbia population density of the cities examined). The pairing of an intensely rotating storm [i.e., ≥70-kt (36 m s^{-1}) V_{rot}] in a favorable environment for tornadic supercells (i.e., STP80km ≥ 6) was examined in relation to different population densities (Figs. 9 and 10). Different population density exceedance thresholds were tested (i.e., from 0 people km^{-2} to 50 people km^{-2} in intervals of 5). The population density exceedance testing indicated much of the benefit attributed to population density occurred when there was a transition from no population to population density

approaching the threshold for the lowest exurbia population density of Sutton et al. (2006)'s list of 49 major U.S. cities. Beyond that threshold, there was decreasing value as a result of reduced sample size. Using a 20 people km^{-2} threshold offered a blend of strong discriminatory value while maintaining a relatively robust sample size for rare events. Using both the lower bound of exurbia population density from Sutton et al. (2006) as a guide and population density's relationship to peak DI-estimated wind speed as a basis for discerning damage intensity, the population density threshold was set at 20 people km^{-2}.

Many variables can potentially influence tornado damage (or lack thereof) and resultant peak DI-estimated wind speeds, though the most intense tornadoes generally pose the greatest threat to life and property. Thus, the highest combination of V_{rot} and STP80km [i.e., ≥70 kt (36 m s^{-1}) and ≥6] was additionally stratified by population density ≥ 20 people km^{-2} (Figs. 9–12). The interquartile ranges between level-4 (lower population density) and level-5 (higher population density) were almost completely offset (Figs. 9 and 12), and the median peak DI wind speed difference was 30 mph (13 m s^{-1}). The minor difference in the median V_{rot} [5 kt (3 m s^{-1})] and STP80km (0.6) between level 4 and 5 (Fig. 12) suggests that the difference in population density is the *primary* influencing factor in the difference in the peak DI wind speeds between the level-4 and level-5 groups.

The peak DI wind speed distributions for levels 2–5 were offset by roughly one quartile (comparing adjacent levels) and the interquartile ranges between levels 1 and 3, 2 and 4, and 3 and 5 are largely offset—indicative of an ability to distinguish between ±2 levels (Fig. 12). Additionally, the median values of STP80km increased from 0.8 to 10.1 from the level-1 to the level-4 groups.

The different IBW tornado warning tiers (i.e., base-tier, considerable, catastrophic) were compared using V_{rot} and peak DI-estimated wind speeds during the IBW era (i.e., 2012–17; Figs. 5, 8, and 12). The base-tier tornado warning median values for V_{rot} and peak DI-estimated wind speed [38 kt (95 mph)] were the weakest values among tornado warning types. Considerable-tag and catastrophic-tag IBW tornado warning median values for V_{rot} and peak DI-estimated wind

Level	STP80km	Vrot (kt)	Pop. density (people km^{-2})	Wind Speed (mph) Damage Estimate	0.5° DI scans within WSDE {Independent}	Wind speed median (mph) {Independent}	Independent Mean Absolute Error (mph)	Independent Variance (S)
5	≥ 6.0	≥ 70	≥ 20	140 – 205	84% {75%}	170 {149}	2.9	282
4	≥ 6.0	≥ 70	< 20	110 – 180	82% {80%}	140 {130}	3.9	535
3	1.0 – 5.9	≥ 70		100 – 170	80% {84%}	122 {127}	1.8	552
3	≥ 3.0	50 – 69		90 – 165	81% {84%}	110 {107}	2.1	472
2	≥ 3.0	25 – 49		75 – 145	89% {87%}	97 {95}	0.8	292
2	< 1.0	≥ 40		75 – 140	87% {100%}	97 {103}	0	128
2	1.0 – 2.9	25 – 69		75 – 135	86% {83%}	95 {93}	1.0	311
1	< 1.0	< 40		60 – 110	96% {99%}	88 {90}	0.1	150
1	≥ 1.0	< 25		60 – 110	95% {94%}	88 {85}	0.4	201

FIG. 10. Calibrated tornado potential damage intensity levels and peak DI wind speed damage estimate (WSDE), consisting of combinations of V_{rot} (kt), STP80km, and population density (people km^{-2}). Percentage of 0.5° DI scans within the WSDE and median wind speed (mph) of each criterion is provided (independent sample in brackets). The independent mean absolute error (mph) and variance are in the rightmost columns. The colors correspond to the levels 1–5 in Fig. 9 (1 mph = 0.447 m s^{-1}, 1 kt = 0.514 m s^{-1}).
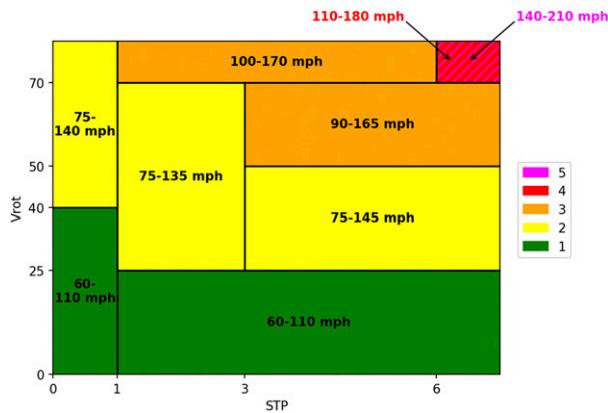
FIG. 11. As in Fig. 10, but for wind speed ranges (mph; labeled) mapped using STP80km (*x* axis) and V_{rot} (*y* axis) based on combinations of V_{rot} (kt), STP80km, and population density (people km^{-2}). Colors for the different levels are provided in the legend to the right (1 mph = 0.447 m s^{-1}, 1 kt = 0.514 m s^{-1}).

speed were markedly stronger [51 kt (26 m s^{-1}), 107 mph (48 m s^{-1}); 62 kt (32 m s^{-1}), 120 mph (54 m s^{-1}) respectively], matching the intent of IBW and supporting the notion that NWS meteorologists are able to discriminate between weaker and more intense damage-based tornado wind speeds, as represented by V_{rot} and the near-storm environment. Furthermore,

the IBW data were also compared to the larger dataset (i.e., 2009–17) of V_{rot} and peak DI wind speeds (Fig. 12). The median values of V_{rot} and peak DI wind speed with the base-tier IBW tornado warnings nearly matched our proposed level-2. The median values of level-1 were weaker than base-tier warnings, but level-4 and level-5 values were much stronger than considerable-tag or catastrophic-tag IBW median values. In summary, the proposed level 1–5 data-driven approach, utilizing V_{rot}, STP80km, and population density, allows potentially greater discrimination of tornado intensity than the three IBW tornado warning tiers (median values of level 1–5 span a DI wind speed range of 82 mph versus only 25 mph for the IBW median values).

d. Independent test sample

A smaller independent dataset containing 2263 0.5° DI scans from 2019 to 2020 was compared to the 7513 0.5° DI scans from the larger dataset from 2009 to 2017 for the level 1–5 data-driven approach using V_{rot}, STP80km, and population density (Figs. 10, 13, and 14). The distributions of peak DI-based wind speed from the 9 different combination ranges of V_{rot}, STP, and population density were evaluated. Considerable overlap of the interquartile ranges is evident for most of the level-1–3 parameter combinations (Fig. 13). The independent sample's peak DI wind speeds were weaker across their distributions for the level-4 and level-5 0.5° DI scans, but it is uncertain whether the independent sample is considerably different due to limited
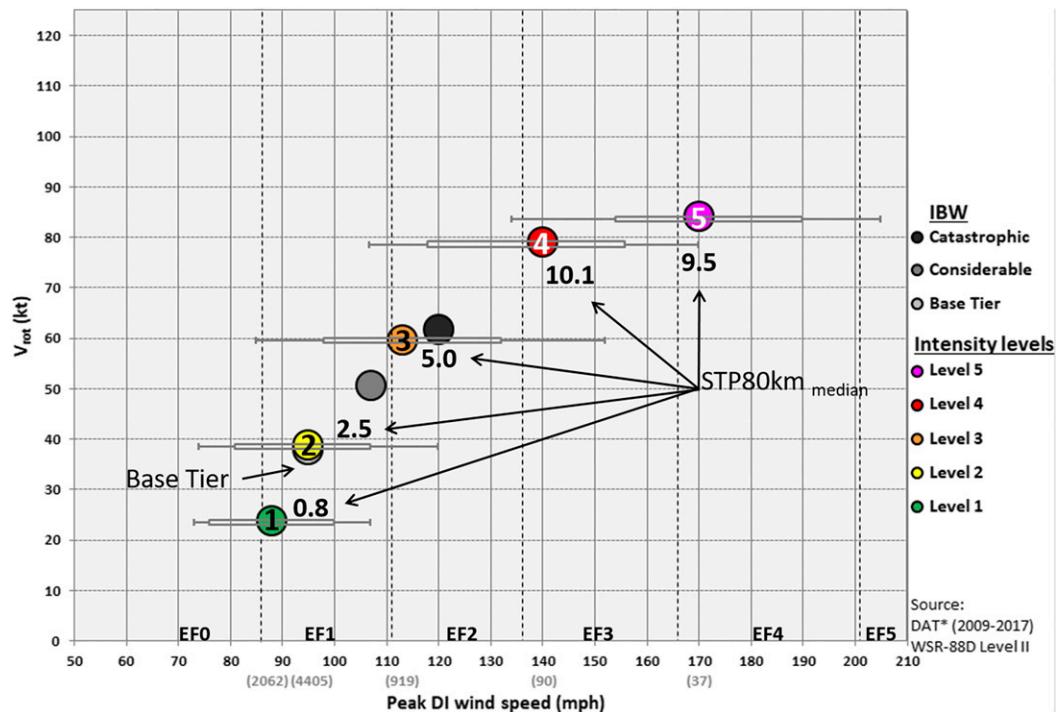
FIG. 12. The median values (circles) of peak DI wind speed (mph; *x* coordinate) and V_{rot} (kt; *y* coordinate) for the existing IBW tornado warning tiers (base, considerable, and catastrophic) vs calibrated tornado potential damage intensity levels 1–5. Box-and-whisker plot of peak DI wind speed by levels 1–5; the hollow boxes span from the 25th to the 75th percentile, the whiskers extend to the 90th and to the 10th percentiles, and sample sizes for each level are shown in parentheses (1 mph = 0.447 m s^{-1}, 1 kt = 0.514 m s^{-1}).
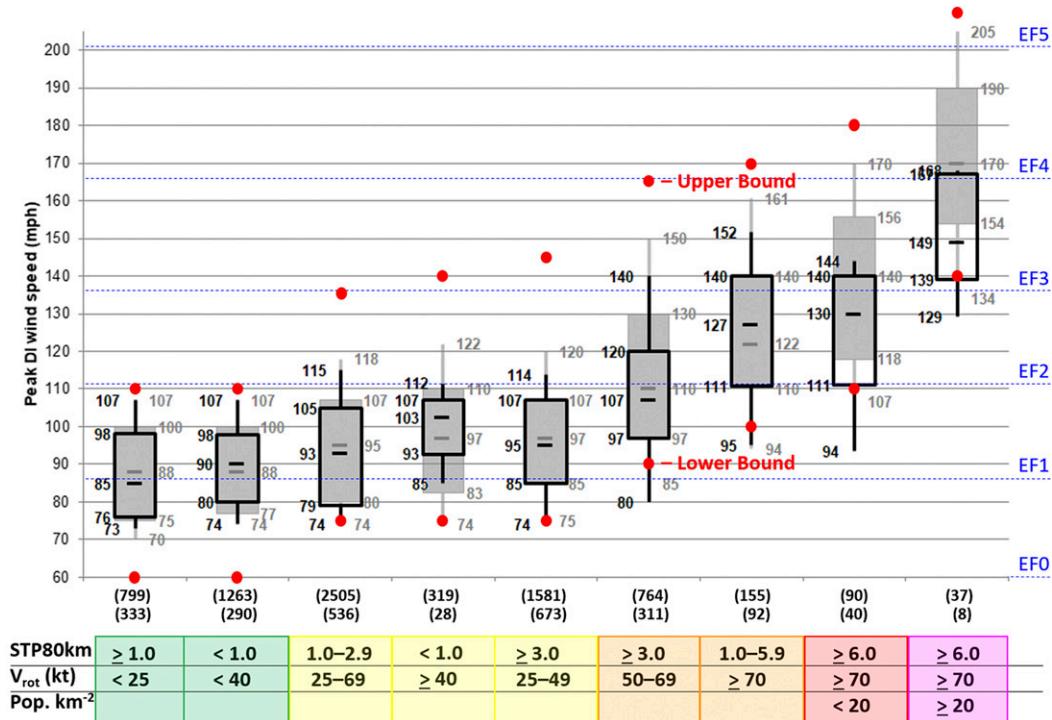
FIG. 13. Box-and-whisker plot of peak damage indicator (DI) wind speed (mph) by 0.5° DI scan ≤ 10 000 ft above radar level for corresponding to rows of criteria in (x axis) vs peak DI wind speed (mph; y axis) (2009–17 data are shaded gray, labels on right). Black overlays (labels on left) denote 2019–20 data. The 10th, 25th, median, 75th, and 90th percentiles are annotated. The red circles are the lower and upper bounds of the peak DI wind speed damage estimate (WSDE) for each category shown in Figs. 9 and 10. Sample sizes (bottom) for each set of criteria are shown in parentheses [(top) 2009–17 and (bottom) 2019–20]. The colors correspond to the levels 1–5 in Figs. 9 and 10 (1 mph = 0.447 m s^{-1}, 1 kt = 0.514 m s^{-1}).

sample size on the high-end of the scale, both in terms of V_{rot} and EF4+ DIs. The independent sample's level-3–5 0.5° DI scans exhibited the largest mean absolute error (Fig. 10) and generally had higher variance.

The peak V_{rot} located anywhere along the entire tornado path [i.e., Smith et al. (2015) approach], in which the peak V_{rot} may not necessarily match with the peak DI-estimated wind speeds, was also evaluated between the independent and larger datasets. An exceedance peak V_{rot} display (Fig. 14)[4] enables an analysis of threshold values of V_{rot} during an ongoing tornado. There is little slope to the probability curves from the 0+- to 20+-kt exceedance bins in Fig. 14, which suggests high confidence that the clear majority of peak DI wind speed estimates will be weak (<110 kt). The slope of the probability curves increases notably as peak V_{rot} exceedance increases from 20+ to 60+ kt, with a correspondingly large increase (~10% at 20+ V_{rot} to >50% at 60+ V_{rot}) in the probabilities of 125+ mph peak DI wind speeds. The probabilities of the most extreme DI

wind speeds become substantial as peak V_{rot} increases above 70 kt. For example, consider a V_{rot} signature for an ongoing tornado that strengthens from 55 kt (28 m s^{-1}) to 75 kt (39 m s^{-1}). Per Fig. 14, the probability of a 140+-mph (63 m s^{-1}) peak DI-estimated wind speed for the entire tornado path increases from 20%–24% to 54%–60%, based on both 2009–17 data and the smaller independent sample. The exceedance probability distributions with the independent sample were within 5%–10% of Part I sample, especially where both samples were relatively large [i.e., V_{rot} up to 70+ kt (36 m s^{-1})].

e. Duration

The durations of tornadoes with $V_{rot} \geq 70$ kt in environments of STP80km ≥ 6 were compared for cases with the entire path affecting areas of low population density (i.e., <20 people km^{-2}), versus a mutually exclusive sample of tornadoes with one or more 0.5° DI scans in areas ≥ 20 people km^{-2} (Fig. 15). The low-population-density tornadoes, with <15 min of combined $V_{rot} \geq 70$ kt in environments of STP80km ≥ 6, had entire-path peak wind speed distributions that were comparable to the level-4 distribution (i.e., scan-by-scan basis in Fig. 13). However, once a low-population-density tornadic storm exceeded 15 min of these criteria, higher final-rating peak estimated wind speeds become more probable (i.e., upper half of the level-4 distribution). The highest final-rating peak

---

[4] The data in Fig. 14 represent the peak values for the entire tornado path. The sample size differences (637 tornadoes in section 2a and 615 tornadoes in Fig. 14) are the result of incomplete data for 22 of the tornadoes, such as missing radar data or 0.5° scans above 10 000 ft ARL.
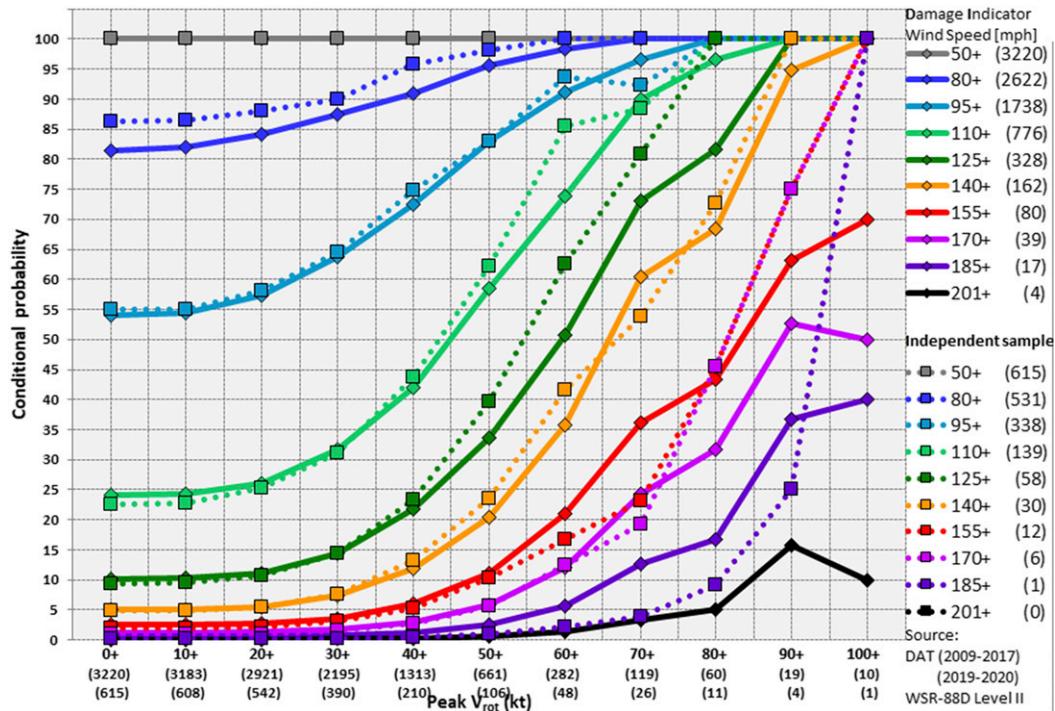
FIG. 14. Conditional probability of peak DI wind speed exceedance (legend) for an entire tornado binned for peak $0.5°$ scan rotational velocity (peak V_{rot}) [kt; x coordinate, (sample size)] anywhere along a tornado path [2009–17, solid line; 2019–20, dotted line; from ≤10 000 ft (3048 m) above radar level (ARL); 1 mph = 0.447 m s^{-1}, 1 kt = 0.514 m s^{-1}].

estimated wind speeds were associated with tornadoes impacting population footprints with ≥20 people km^{-2} with the same STP80km ≥ 6, V_{rot} ≥ 70 kt criteria. Tornadoes with 1–5-min durations in population density ≥ 20 people km^{-2} exhibited a similar distribution in the 10th–75th percentile values to the level-5 events. However, as duration increased into the 6–15- and the ≥15-min groupings, the distributions for the final-rating peak estimated wind speeds increased. The data presented here suggest that peak DI-estimated wind speeds increase (for an entire tornado lifetime) as the duration of high-end V_{rot} (≥70 kt) increases in an environment very favorable for tornadic supercells (e.g., STP80km ≥ 6), but sample sizes are small. It is important to note that the mean values of V_{rot}, STP80km, and duration were 81 kt, 8.8, and 9 min, respectively, for the tornadoes in Fig. 15 that never encountered ≥20 people km^{-2}, compared to 93 kt, 10.0, and 25 min, respectively, for the tornadoes that impacted areas with ≥20 people km^{-2} somewhere along their path. Thus, final-rating peak DI wind speeds of EF3+ tornadoes appear to be related to a combination of relatively long durations of large V_{rot} in environments strongly favoring tornadic supercells, and interaction with areas of higher population density (i.e., greater DoD DI availability).

4. Discussion

Ernst et al. (2018) described the desire by emergency managers to receive additional information from forecasters describing tornado intensity/impact and uncertainty in order to better respond to a real-time tornado event before damage survey results are completed. Although the need described by Ernst et al. (2018) preceded IBW, the three IBW tornado warning tiers offer a first formal attempt at indirect damage intensity forecasts for tornadoes and provide additional information that can be used by emergency managers and broadcast meteorologists. The probability distribution for each V_{rot}/STP80km combination yields probabilities for each EF rating (not shown), but identifying an individual EF-scale rating on a $0.5°$ radar scan basis will likely prove difficult. However, the use of exceedance probabilities (Fig. 16) provides more utility to differentiate between the different V_{rot}/STP80km combinations for higher EF ratings. For example, a tornadic storm that reaches level-5 criteria for at least one $0.5°$ radar scan corresponds to an 87.5% (or 7 out of 8 chance) of the tornado later becoming rated as violent (i.e., EF4–5). Moreover, application of this information can address value-proposition decision making, which enables different users to select different probabilistic thresholds.

Prior efforts to improve tornado warning lead time have focused primarily on discrimination between weak (EF0–EF1) and significant (EF2+) tornadoes, or lead time for the onset of significant (EF2+) tornado damage, which is related to the application of the considerable and catastrophic IBW tags. The IBW tags are qualitative in nature, which leaves a quantitative gap in the NWS tornado warning program. Incorporating peak wind speed or EF-scale ranges (to account for inherent uncertainty) into tornado warnings, in addition to and support of the qualitative IBW tags, appears plausible based on the results of this work and Part I. A pivot toward reproducible decision
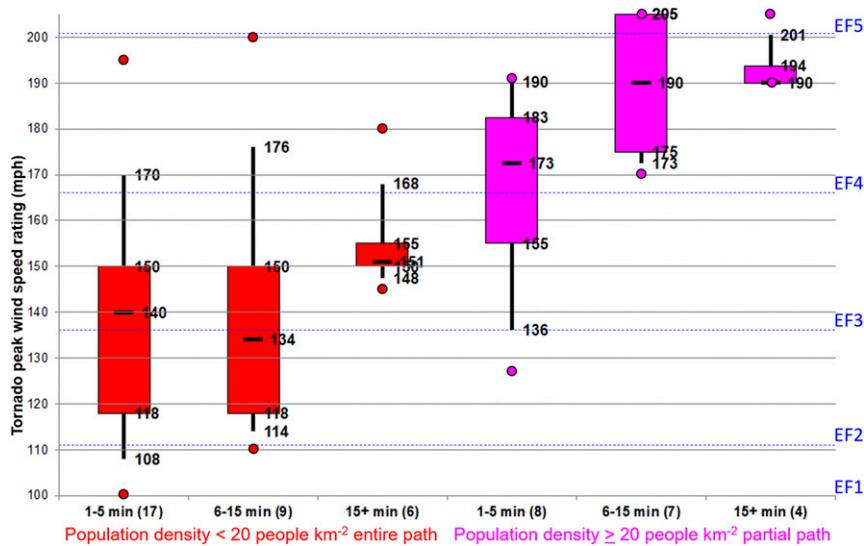
FIG. 15. Box-and-whisker plot of peak damage-estimated wind speed (mph) by population density and duration (min) of $V_{rot} \geq 70$ kt with STP80km ≥ 6. Tornadoes with population density < 20 people km^{-2} during their entire paths are plotted in the red boxes, and the sum of the duration of individual scans where population density was >20 people km^{-2} for a mutually exclusive sample of tornadoes are plotted in the magenta boxes. The 10th, 25th, median, 75th, and 90th percentiles are annotated with minimum and maximum values (circles). Sample sizes (bottom) for combined events from 2009–17 and 2019–20 samples. All five of the EF5 tornadoes' wind speeds were adjusted to 205 mph (1 mph = 0.447 m s^{-1}, 1 kt = 0.514 m s^{-1}).

aids like V_{rot}/STP/population density could contribute both value and consistency in operational decision-making regarding tornadoes, through the addition of quantitative information regarding potential tornado intensity. A potential transitional step in the warning process could initially focus on targeting stronger tornado events (i.e., level 3–5) and quantifying the diagnostic basis for considerable and catastrophic IBW tags, in scenarios posing the greatest threat to life and property. Both tornado warnings and severe weather statements can provide important nuances describing tornado intensity variations within tornado warnings, and help improve downstream expectations and reactions.

With this dataset, quantification of IBW tags is possible based on relatively simple combinations of the V_{rot} and STP80km criteria. An evidence-based and expanded version of IBW can provide additional information on the real-time tornado intensity risk by adding levels within the weak and intense parts of the tornado intensity spectrum. The different combination groups of V_{rot}/STP80km, which are remotely sensed or estimated in real time, correspond to a 1–5 level of potential tornado damage intensity scale (Fig. 12)—similar to the existing Saffir–Simpson category 1–5 scale used for hurricanes. In addition to providing a familiar type of scale in levels 1–5, the explicit wind speed estimates can help to remove any doubt as to whether level 5 is more serious than level 1. An increase in V_{rot}/STP80km-based levels is related to an accompanying propensity for higher SPC convective outlook tornado probabilities and more significant watch type (not shown). Implementing such a change and proposing guidelines (e.g., Figs. 10 and 11) for a best-practices approach to describe tornado risk is congruent with both scientific and

communication goals of NOAA's FACETs (Rothfusz et al. 2018) vision.

5. Summary and forecaster notes

In Part I, we developed a large sample of tornadoes with both individual DIs from the DAT and corresponding WSR-88D 0.5° V_{rot}, and demonstrated that V_{rot} and near-storm environment (STP80km) can be combined to estimate peak DI wind speeds on a scan-by-scan basis with WSR-88D data. This work extends the findings of Part I to develop an application to IBW for ongoing tornadoes by combining V_{rot} and STP80km into a five-level scale for expected tornado intensity within tornado warnings. Based on the input parameters of V_{rot} and the maximum neighborhood value of STP, the intensity scale maps out expected ranges of peak tornado wind speeds that increase as both V_{rot} and STP80km increase. The more common combinations of relatively weak V_{rot} (<40 kt) and low STP (<1) result in peak tornado wind speed estimates ≤ 110 mph (EF0–EF1 damage). Peak tornado wind speed estimates increase into the EF2–EF3 range (115–145 mph) for midrange combinations of V_{rot} (~ 45–65 kt) and STP (~ 1–3; corresponding primarily to levels 2–3 in Figs. 9 and 10). Violent tornadoes (EF4+ damage and peak wind speeds ≥ 166 mph) become a possibility for the high-end V_{rot} (≥ 70 kt) and STP80km (≥ 6) combinations. The expected value of the proposed scale will be to provide simple and reproducible estimates of tornado intensity in real time, with potential applications within the framework of IBW.

Consistent real-time application of the suggested five-level scale, within the context of tornado warning time
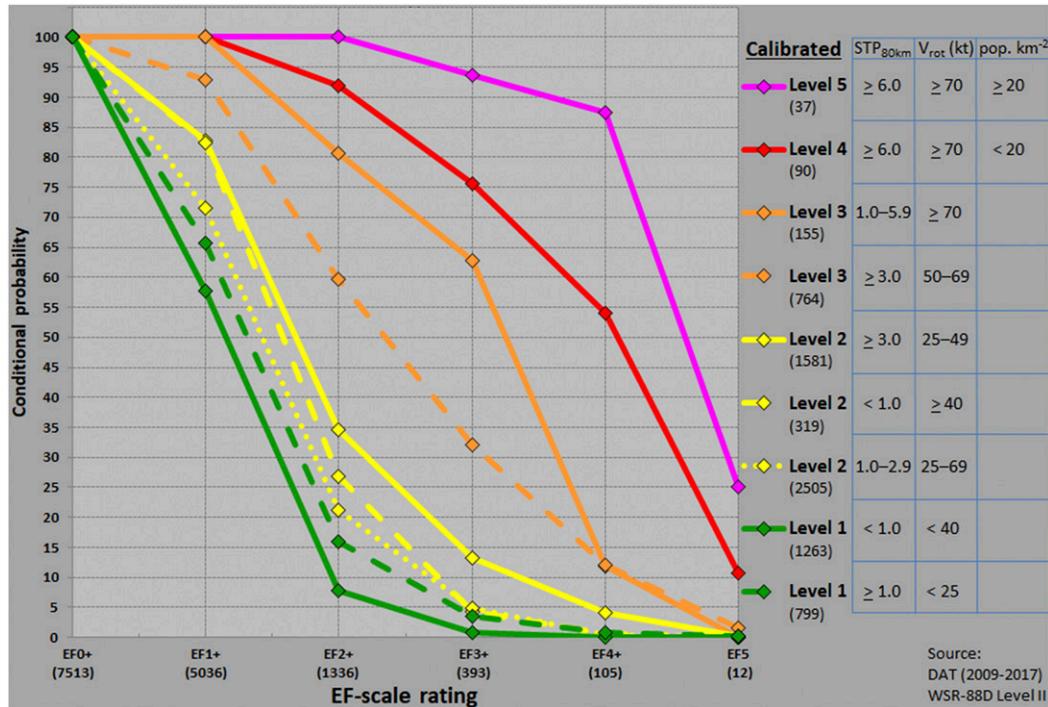
FIG. 16. Conditional probability (*y* coordinate) by EF-scale exceedance rating (*x* coordinate, sample size in parentheses) for different combinations of STP80km, V_{rot} (kt), and population density (people km^{-2}) corresponding to level 1–5 values (legend, right; 1 mph = 0.447 m s^{-1}, 1 kt = 0.514 m s^{-1}).

scales, may ultimately depend on a combination of factors. Three critical factors in estimating tornado probabilities (in the absence of direct evidence of an ongoing tornado) are as follows:

1) Proper interpretation of velocity (V_{rot}) data to avoid known concerns such as sidelobe contamination (Piltz and Burgess 2009), improper dealiasing, and range folded data.
2) Incorporation of unconditional tornado (EF0+) probabilities in the lower portions of the V_{rot} distribution, potentially accounting for the effects of circulation diameter and radar range (e.g., T17).
3) Incorporation of nonconvectively contaminated, near-storm environment information (e.g., maximum STP value within an 80-km radius).

Additional considerations for explicit peak tornado intensity estimates are:

4) Generally more than one V_{rot} scan as a basis for decisions, especially for suspected high-impact tornadoes.
5) High-confidence, corroborating evidence of an ongoing tornado (TDS or spotter reports).

The rare combination of criteria constituting a level-5 event (i.e., extreme V_{rot} [≥70 kt (36 m s^{-1})], a very favorable environment (STP80km ≥ 6), and a population center with an imminent tornado impact) is designed to help identify the likelihood of extreme tornado damage with peak DI wind speeds in the EF4–EF5 range [e.g., ≥170 mph (76 m s^{-1})]. As the duration of these high-end events increases (extreme V_{rot}

in a large STP environment), the odds increase that an intense tornado will be revealed via surveyed damage, especially in more densely populated areas. The research to operations (R2O) application of this work spans the construction of the level 1–5 methodology and bridges the gap to the operational community tasked with real-time identification of rare-event forecasting, and enables meteorologists the opportunity to provide consistent and credible messaging of rare ongoing events.

REFERENCES

Anderson-Frey, A. K., Y. P. Richardson, A. R. Dean, R. L. Thompson, and B. T. Smith, 2016: Investigation of near-storm environments for tornado events and warnings. *Wea. Forecasting*, **31**, 1771–1790, https://doi.org/10.1175/WAF-D-16-0046.1.
——, ——, ——, ——, and ——, 2018: Near-storm environments of outbreak and isolated tornadoes. *Wea. Forecasting*, **33**, 1397–1412, https://doi.org/10.1175/WAF-D-18-0057.1.

Baerg, B. M., and Coauthors, 2020: Radar-based, storm-scale circulation and tornado-probability tendencies preceding tornadogenesis in Kansas and Nebraska. *Electron. J. Severe Storms Meteor.*, **15** (3), https://ejssm.org/ojs/index.php/ejssm/article/viewArticle/179.

Blair, S. F., and J. W. Leighton, 2014: Assessing real-time tornado information disseminated through NWS products. *Wea. Forecasting*, **29**, 591–600, https://doi.org/10.1175/WAF-D-13-00126.1.

Bluestein, H. B., K. J. Thiem, J. C. Snyder, and J. B. Houser, 2018: The multiple-vortex structure of the El Reno, Oklahoma, tornado on 31 May 2013. *Mon. Wea. Rev.*, **146**, 2483–2502, https://doi.org/10.1175/MWR-D-18-0073.1.

——, ——, ——, and ——, 2019: Tornadogenesis and early tornado evolution in the El Reno, Oklahoma, supercell on 31 May 2013. *Mon. Wea. Rev.*, **147**, 2045–2066, https://doi.org/10.1175/MWR-D-18-0338.1.

Brady, R. H., and E. J. Szoke, 1989: A case study of non-mesocyclone tornado development in northeast Colorado: Similarities to waterspout formation. *Mon. Wea. Rev.*, **117**, 843–856, https://doi.org/10.1175/1520-0493(1989)117<0843:ACSONT>2.0.CO;2.

Camp, P. J., K. Stellman, and J. Settelmaier, 2010: Utilizing mobile devices for enhanced storm damage surveys. *26th Conf. on Interactive Information and Processing Systems (IIPS) for Meteorology, Oceanography, and Hydrology*, Atlanta, GA, Amer. Meteor. Soc., 5B.4, https://ams.confex.com/ams/90annual/techprogram/paper_161540.htm.

Cohen, A. E., J. B. Cohen, R. L. Thompson, and B. T. Smith, 2018: Simulating tornado probability and tornado wind speed based on statistical models. *Wea. Forecasting*, **33**, 1099–1108, https://doi.org/10.1175/WAF-D-17-0170.1.

Edwards, R., A. R. Dean, R. L. Thompson, and B. T. Smith, 2012: Convective modes for significant severe thunderstorms in the contiguous United States. Part III: Tropical cyclone tornadoes. *Wea. Forecasting*, **27**, 1507–1519, https://doi.org/10.1175/WAF-D-11-00117.1.

Ernst, S., D. Ladue, and A. Gerard, 2018: Understanding emergency manager forecast use in severe weather events. *J. Oper. Meteor.*, **6**, 95–105, https://doi.org/10.15191/nwajom.2018.0609.

French, M. M., H. B. Bluestein, I. PopStefanija, C. A. Baldi, and R. T. Bluth, 2013: Reexamining the vertical development of tornadic vortex signatures in supercells. *Mon. Wea. Rev.*, **141**, 4576–4601, https://doi.org/10.1175/MWR-D-12-00315.1.

——, ——, ——, ——, and ——, 2014: Mobile, Phased-array, Doppler radar observations of tornadoes at X band. *Mon. Wea. Rev.*, **142**, 1010–1036, https://doi.org/10.1175/MWR-D-13-00101.1.

Gibbs, J. G., 2016: A skill assessment of techniques for real-time diagnosis and short-term prediction of tornado intensity using the WSR-88D. *J. Oper. Meteor.*, **4**, 170–181, https://doi.org/10.15191/nwajom.2016.0413.

——, and B. R. Bowers, 2019: Techniques and thresholds of significance for using WSR-88D velocity data to anticipate significant tornadoes. *J. Oper. Meteor.*, **7**, 117–137, https://doi.org/10.15191/nwajom.2019.0709.

Kingfield, D. M., and J. G. LaDue, 2015: The relationship between automated low-level velocity calculations from the WSR-88D and maximum tornado intensity determined from damage surveys. *Wea. Forecasting*, **30**, 1125–1139, https://doi.org/10.1175/WAF-D-14-00096.1.

Marquis, J., Y. Richardson, P. Markowski, J. Wurman, K. Kosiba, and P. Robinson, 2016: An investigation of the Goshen County, Wyoming, tornadic supercell of 5 June 2009 using EnKF assimilation of mobile mesonet and radar observations collected during VORTEX2. Part II: Mesocyclone-scale processes affecting tornado formation, maintenance, and decay. *Mon. Wea. Rev.*, **144**, 3441–3463, https://doi.org/10.1175/MWR-D-15-0411.1.

Piltz, S. F., and D. W. Burgess, 2009: The impacts of thunderstorm geometry and WSR-88D beam characteristics on diagnosing supercell tornadoes. *34th Conf. on Radar Meteorology*, Williamsburg, VA, Amer. Meteor. Soc., P6.18, https://ams.confex.com/ams/34Radar/techprogram/paper_155944.htm.

Rothfusz, L. P., R. Schneider, D. Novak, K. Klockow-McClain, A. E. Gerard, C. Karstens, G. J. Stumpf, and T. M. Smith, 2018: FACETs: A proposed next-generation paradigm for high-impact weather forecasting. *Bull. Amer. Meteor. Soc.*, **99**, 2025–2043, https://doi.org/10.1175/BAMS-D-16-0100.1.

Sessa, M. F., and R. J. Trapp, 2020: Observed relationship between tornado intensity and pretornadic mesocyclone characteristics. *Wea. Forecasting*, **35**, 1243–1261, https://doi.org/10.1175/WAF-D-19-0099.1.

Smith, B. T., R. L. Thompson, J. S. Grams, C. Broyles, and H. E. Brooks, 2012: Convective modes for significant severe thunderstorms in the contiguous United States. Part I: Storm classification and climatology. *Wea. Forecasting*, **27**, 1114–1135, https://doi.org/10.1175/WAF-D-11-00115.1.

——, ——, A. R. Dean, and P. T. Marsh, 2015: Diagnosing the conditional probability of tornado damage rating using environmental and radar attributes. *Wea. Forecasting*, **30**, 914–932, https://doi.org/10.1175/WAF-D-14-00122.1.

——, ——, D. A. Speheger, A. R. Dean, C. D. Karstens, and A. K. Anderson-Frey, 2020: WSR-88D Tornado Intensity Estimates. Part I: Real-Time Probabilities of Peak Tornado Wind Speeds. *Wea. Forecasting*, **35**, 2479–2492, https://doi.org/10.1175/WAF-D-20-0010.1.

Sutton, P. C., T. J. Cova, and C. D. Elvidge, 2006: Mapping "Exurbia" in the conterminous United States using nighttime satellite imagery. *Geocarto Int.*, **21**, 39–45, https://doi.org/10.1080/10106040608542382.

Thompson, R. L., B. T. Smith, J. S. Grams, A. R. Dean, and C. Broyles, 2012: Convective modes for significant severe thunderstorms in the contiguous United States. Part II: Supercell and QLCS tornado environments. *Wea. Forecasting*, **27**, 1136–1154, https://doi.org/10.1175/WAF-D-11-00116.1.

——, and Coauthors, 2017: Tornado damage rating probabilities derived from WSR-88D data. *Wea. Forecasting*, **32**, 1509–1528, https://doi.org/10.1175/WAF-D-17-0004.1.

Wagenmaker, R., G. Mann, and M. Hudson, 2014: NWS Central Region Impact-Based Warning project introduction and overview. NOAA.

Wakimoto, R. M., and Coauthors, 2016: Aerial damage survey of the 2013 El Reno tornado combined with mobile radar data. *Mon. Wea. Rev.*, **144**, 1749–1776, https://doi.org/10.1175/MWR-D-15-0367.1.

WSEC, 2006: A recommendation for an enhanced Fujita scale (EF-scale). Wind Science and Engineering Center, Texas Tech University, 95 pp., http://www.depts.ttu.edu/weweb/EFScale.pdf.